Journal of Computational Physics 229 (2010) 5246–5256

Contents lists available at ScienceDirect

Journal of Computational Physics

journal homepage: www.elsevier.com/locate/jcp

A multi-phase level set framework for source reconstruction in bioluminescence tomography

Heyu Huang [a], Xiaochao Qu [a], Jimin Liang [a], Xiaowei He [a,c], Xueli Chen [a], Da'an Yang [a], Jie Tian [a,b,*]

[a] Life Sciences Research Center, School of Life Sciences and Technology, Xidian University, Xi'an, Shaanxi 710071, China
[b] Institute of Automation, Chinese Academy of Sciences, Beijing 100190, China
[c] School of Information Science and Technology, Northwest University, Xi'an 710069, China

ARTICLE INFO

Article history:
Received 14 July 2009
Received in revised form 10 January 2010
Accepted 26 March 2010
Available online 1 April 2010

Keywords:
Bioluminescence tomography
Multi-phase level set
Inverse reconstruction

ABSTRACT

We propose a novel multi-phase level set algorithm for solving the inverse problem of bioluminescence tomography. The distribution of unknown interior source is considered as piecewise constant and represented by using multiple level set functions. The localization of interior bioluminescence source is implemented by tracing the evolution of level set function. An alternate search scheme is incorporated to ensure the global optimal of reconstruction. Both numerical and physical experiments are performed to evaluate the developed level set reconstruction method. Reconstruction results show that the proposed method can stably resolve the interior source of bioluminescence tomography.

1. Introduction

Optical molecular imaging has attracted extensive attention in the last decade due to its ability of non-invasive visualization of specific molecular targets, pathways and physiological effects *in vivo*. This technique is widely considered to be used for early disease diagnosis, tumor cell detection and drug development [1,2]. As an optical molecular imaging modality, bioluminescence tomography (BLT) can inversely recover the luminescence sources embedded in biological tissue with sensitive charge-coupled device (CCD) camera capturing the surface light signals [3]. BLT does not require external source for excitation and the inherent background noise is quite low, so it is widely studied for live small animal imaging [3–5].

The study of photon propagation in biological tissue is the prerequisite for BLT reconstruction. Generally, the propagation process is modeled as a radiative transfer equation (RTE) [6]. Solving the integro-differential equation is of high complexity and time consuming. Some approximate models have been developed to simplify this equation, such as high-order approximation [6,7] and phase approximation [8]. Because the biological tissue exhibits high scattering characteristic for near infrared photons, diffusion equation, a first-order approximation of RTE, has been widely used in the simulation of near infrared imaging [9–11]. Finite element method (FEM), which can handle solving domains of arbitrary geometry, is commonly used for solving diffusion approximate equations [12–16]. During the solving procedure, the relationship between the interior source and the surface flux density is established accurately, which can contribute to the reconstruction of bioluminescent source.

The inverse reconstruction of bioluminescence source is an ill-posed problem. Approximate solution which minimizes a given objective function is widely accepted as the reconstruction result. Iteration and optimization methods are generally employed to find the approximate solution [14–18]. At present, the presentation of source distribution in most of the

* Corresponding author at: Life Sciences Research Center, School of Life Sciences and Technology, Xidian University, Xi'an, Shaanxi 710071, China. Tel.: +86 10 82618465/86 29 88201842; fax: +86 10 62527995.
E-mail address: tian@ieee.org (J. Tian).

0021-9991/$ - see front matter © 2010 Elsevier Inc. All rights reserved.
doi:10.1016/j.jcp.2010.03.041

FEM based BLT reconstruction methods is in a continuous form, which depends on the nodes or elements of FEM mesh. This processing method is flexible but sensitive to the variation of the measured surface data. Regularization terms, normally Tikhonov–Philips term is usually added to the objective function to improve the stability, but the difficulty of determining the regularization parameters makes this problem more complicated.

Level set method (LSM) has been proved as a promising tool for solving inverse problems associated with shape optimization since its first demonstration by Sethian and Osher in 1988 [19–22]. In medical imaging research field, e.g. positron emission tomography, microwave tomography, electrical impedance tomography, optical tomography, LSM has shown its great potential for localization of interior object [23–27]. In this method, a sufficient smooth level set function, which has the ability to automatically split and merge domain during the reconstruction procedure, is employed to describe the unknown piecewise constant coefficient distribution. With the evolution of level set function, the actual coefficient distribution can be recovered and the interior object can be located. In this paper, we propose a multi-phase level set framework for solving BLT reconstruction problem. Using multiple level set functions, this algorithm introduces a digital representation form for bioluminescence source distribution, which treats the distribution as piecewise constant and represents the source distribution in a more robust way. In addition, an alternate search scheme between the source density and level set function is employed to ensure the global optimization and improve the stability of reconstruction results. Compared with typical applications of the level set method, which highlight its ability of shape recovery, the application in this contribution is different. For BLT reconstruction, the unknown interior source is often quite tiny, and it is difficult to distinguish the influences of strong small source and weak large source [28]. As a result, we usually neglect the shape of reconstructed source but concentrate on the localization and quantification problems. Experimental results prove the ability of this proposed multi-phase LSM for source localization and multiple sources resolution in BLT reconstruction.

The paper is organized as follows. In Section 2, we describe the mathematical forward and inverse model of BLT, then the multi-phase level set method for BLT source detection is derived and details of the algorithm are presented. Numerical and physical experiments which demonstrate the performance of the proposed algorithm are presented in Sections 3 and 4. Finally, brief conclusions and discussions are provided in Section 5.

2. Method

2.1. Diffusion approximation of BLT model

A generally used luminescent substance in BLT, e.g. firefly luciferase and fluorescein, is considered to emit light with a wavelength of about 600 nm [29]. At this wavelength, the main type of photon propagation in biological tissue is scattering. The process of photon transmission in small animals' chest tissue can be depicted as a steady-state diffusion approximate equation for simplicity [9]. Robin type boundary condition is incorporated when the experiment is implemented in an ideal environment without incoming light to the body surface [30].

$$-\nabla\cdot(D(\mathbf{r})\nabla\Phi(\mathbf{r}))+\mu_a(\mathbf{r})\Phi(\mathbf{r})=S(\mathbf{r})(\mathbf{r}\in\Omega), \tag{1.1}$$

$$\Phi(\mathbf{r})+2A(\mathbf{r};n,n')D(\mathbf{r})(\mathbf{v}(\mathbf{r})\cdot\nabla\Phi(\mathbf{r}))=0(\mathbf{r}\in\partial\Omega), \tag{1.2}$$

where Ω and $\partial\Omega$ are the solving domain and its boundary, $\Phi(\mathbf{r})$ represents the photon flux density (W/mm^2), $S(\mathbf{r})$ is the source energy density (W/mm^3). $\mu_a(\mathbf{r})$ is the absorption coefficient (mm^{-1}) and $\mu_s(\mathbf{r})$ the scattering coefficient (mm^{-1}), $\mathbf{v}(\mathbf{r})$ denotes the unit outer normal on boundary. $D(\mathbf{r})=1/(3(\mu_a(\mathbf{r})+\mu_s'(\mathbf{r})))$ is the optical diffusion coefficient and g is the anisotropy parameter, $\mu_s'(\mathbf{r})=(1-g)\mu_s(\mathbf{r})$ indicates the reduced scattering coefficient (mm^{-1}). $A(\mathbf{r};n,n')$ is the mismatch coefficient between Ω and its surrounding medium, it can be approximately represented as $A(\mathbf{r},n,n')\approx(1+R(\mathbf{r}))/(1-R(\mathbf{r}))$, where n is the refractive index of Ω and n' is refractive index of the surrounding medium. When the experiment is operated in the air, n' is close to 1.0, and $R(\mathbf{r})\approx-1.4399n^{-2}+0.7099n^{-1}+0.6681+0.0636n$ [30]. The measured quantity on the boundary is given by the outgoing radiation [15] as:

$$Q(\mathbf{r})=-D(\mathbf{r})(\mathbf{v}(\mathbf{r})\cdot\nabla\Phi(\mathbf{r}))=\frac{\Phi(\mathbf{r})}{2A(\mathbf{r};n,n')}\quad(\mathbf{r}\in\partial\Omega). \tag{2}$$

Generally, the forward model of BLT defined by (1.1) and (1.2) is solved numerically [12–16,31]. In this paper, we use finite element method to discretely approach the solving domain, and establish the relation between the unknown source distribution and the flux density on the surface. So the data on the surface is calculated as:

$$\Phi^c=F(S), \tag{3}$$

where F is the mapping operator from source distribution to surface flux density. More details of establishing the relationship by using finite element method can be found in [14]. Mismatch between the calculated result Φ^c and the measured data Φ^m on the surface is expressed as:

$$R(S)=\Phi^c-\Phi^m=F(S)-\Phi^m. \tag{4}$$

For the *ill-posed* BLT inverse problem, it is not practical to directly solve for S from linear Eq. (3), and optimization method is usually adopted for the reconstruction to find an approximate solution. Least squares objective function based on the mismatch between the measured data and the calculated data is defined as:

$$J = \frac{1}{2}\|R(S)\|^2. \tag{5}$$

The reconstruction of BLT is reduced to determine the source distribution, which minimizes the least squares objective function. In the following section, a multi-phase level set algorithm is used to determine an approximate optimal solution.

2.2. BLT reconstruction using multi-phase level set function

For simplicity of presentation, we assume the solving domain contains two different domains with piecewise constant source density s_1 and s_2, where s_1 and s_2 are two nonnegative real numbers. Ω_1 denotes the sub domain with the source density of s_1 and Ω_2 defines the other sub domain with the source density of s_2. Using a level set function $\varphi(\mathbf{r})$, the solving domain is represented as:

$$\begin{cases} \mathbf{r} \in \Omega_1, & \varphi(\mathbf{r}) < 0, \\ \mathbf{r} \in \Omega_2, & \varphi(\mathbf{r}) > 0, \end{cases} \tag{6}$$

and $\varphi(\mathbf{r}) = 0$ denotes the interface of the two domains. So the source density distribution in the solving domain can be described as [34,35]:

$$S(\mathbf{r}) = \begin{cases} s_1, & \varphi(\mathbf{r}) \leqslant 0, \\ s_2, & \varphi(\mathbf{r}) > 0. \end{cases} \tag{7}$$

By introducing a one dimension Heaviside function $H(\varphi) = \begin{cases} 1, & \text{while } \varphi > 0 \\ 0, & \text{while } \varphi \leqslant 0 \end{cases}$, $S(\mathbf{r})$ can be rewritten as $S(\mathbf{r}) = s_1(1 - H(\varphi)) + s_2 H(\varphi)$ for simplicity.

If the function $S(\mathbf{r})$ has many pieces, multiple level set functions should be used. We assume that we have two level set functions which divide the whole domain into four parts and describe them following Vese and Chan in [32]:

$$\begin{cases} \Omega_1, & \varphi_1 < 0 \quad \text{and } \varphi_2 < 0, \\ \Omega_2, & \varphi_1 < 0 \quad \text{and } \varphi_2 > 0, \\ \Omega_3, & \varphi_1 > 0 \quad \text{and } \varphi_2 < 0, \\ \Omega_4, & \varphi_1 > 0 \quad \text{and } \varphi_2 > 0. \end{cases} \tag{8}$$

Using the Heaviside function, $S(\mathbf{r})$ with four piecewise constant values of source density can be expressed as:

$$S = s_1(1 - H(\varphi_1))(1 - H(\varphi_2)) + s_2(1 - H(\varphi_1))H(\varphi_2) + s_3 H(\varphi_1)(1 - H(\varphi_2)) + s_4 H(\varphi_1)H(\varphi_2). \tag{9}$$

It is obvious that if n level set functions are adopted, the whole domain will be divided into at most 2^n regions. To concisely express the relationship between regions and level set functions, as Chan and Tai detailed in [20], the 2^n regions is presented in a binary formula as $(i-1)_{binary} = (b_1^i, b_2^i, \ldots, b_n^i)$, for $i = 1,2, \ldots 2^n$, where $b_j^i = 0$ or 1. Therefore source distribution can be presented as:

$$S(\mathbf{r}) = \sum_{i=1}^{2^n} s_i \prod_{j=1}^{n} Q_i(\varphi_j), \tag{10}$$

where

$$Q_i(\varphi_j(\mathbf{r})) = \begin{cases} H(\varphi_j(\mathbf{r})), & b_j^i = 1, \\ 1 - H(\varphi_j(\mathbf{r})), & b_j^i = 0. \end{cases} \tag{11}$$

Once the maximum number of level set functions is known, source distribution of whole domain is obtained. Even if the actual level of source density is less than 2^n, the domain can also be represented using n level set functions, and some subdomains will be merged after some steps of evolution.

2.3. Algorithm

With the evolution of level set functions progressing, the minimum of J in (5) can be obtained. The source location is uniquely determined according to the final domain represented by the level set functions. Therefore, how to identify the evolution law of the level set functions becomes important. An artificial time variable t is introduced to represent the evolution of level set function. The evolution trend of level set function related to t is defined as:

$$f_j(\mathbf{r}, t) = \frac{d\varphi_j(\mathbf{r}, t)}{dt}, \tag{12}$$

where $f_j(\mathbf{r},t)$, $(j = 1 \ldots n)$ determined in every time step induces the descent of the objective function. The differential of objective function corresponding to t yields:

$$\frac{dJ}{dt} = \frac{\partial J}{\partial S}\sum_{j=1}^{n}\left(\frac{\partial S}{\partial \varphi_j}\frac{d\varphi_j}{dt}\right) = \frac{\partial J}{\partial S}\sum_{j=1}^{n}\left(\frac{\partial S}{\partial \varphi_j}f_j\right), \tag{13}$$

where

$$\frac{\partial S}{\partial \varphi_j} = \sum_{i=1}^{2^n} s_i \frac{dQ_i(\varphi_j)}{d\varphi_j}\prod_{k=1,k\neq j}^{n} Q_i(\varphi_k), \tag{14}$$

$$\partial J/\partial S = R'(S)^* R(S), \tag{15}$$

where $dQ_i(\varphi_j)/d\varphi_j = \pm\delta(\varphi_j)$, and $\delta(\varphi) = H'(\varphi)$ is the one dimension Dirac delta distribution. R' is the Frechet derivatives of R, R^* is the adjoint operator of R. An acceptable descent direction of J satisfies $dJ/dt \leqslant 0$. Therefore, the direction of $f_j(\mathbf{r},t)$, which satisfies $dJ/dt \leqslant 0$, can be accepted as the descent direction of level set function [21]. Because $\delta(\varphi)$ and s_i are nonnegative, a direction is expressed as:

$$f_j(\mathbf{r},t) = -R'(S)^* R(S)\sum_{i=1}^{2^n} s_i \mathrm{Sign}(dQ_i(\varphi_j)/d\varphi_j)\prod_{k=1,k\neq j}^{n} Q_i(\varphi_k), \tag{16}$$

where $\mathrm{Sign}(x)$ is the signum function, and $\mathrm{Sign}(x) = 1$ when $x > 0$, $\mathrm{Sign}(x) = -1$ when $x < 0$.

Then we obtain the iterative formula of the level set function as:

$$\varphi_j^{(p)} = \varphi_j^{(p-1)} + \tau f_j^{(p)}, \tag{17}$$

where $\varphi_j^{(0)}$ is the initial level set function, τ a positive time step which is set as a fixed value in the following numerical simulation.

For typical BLT reconstruction problem, both source density and position need to be determined. Here we incorporate an alternate search scheme into the aforementioned level set method to avoid simultaneous searching for the two variables. In this scheme, source density of every different level changes independently following a linear rule. For each combination of the source density values, we evolve level set functions to minimize the objective function. Among all the minimums of objective function, the minimal value is considered as the final solution of objective function, and the corresponding density and level set functions as the reconstructed results of BLT. We describe the BLT reconstruction procedure of the alternate search scheme based on a two-phase representation in Fig. 1. Following a linear rule, we steadily increase the source density from s_l to s_u with step length δs, where s_l and s_u are the lower and upper bound of the source density respectively. For every certain source density, according to the descent direction, we search the source location by evolving level set function to approach a minimum of objective function. The minimal value is stored as $J(k)$ and the corresponding level set function stored as $\varphi(k)$. The evolution of level set function stops when the iterative number reaches the pre-set maximum number N or the difference between the value of objective function in adjacent two step is less than a pre-set threshold ε. The minimum of $\{J(1), J(2), \ldots, J(k), \ldots\}$ is taken as the global optimum and the reconstructed source location is indicated by the corresponding level set function.

Although searching source density with a small enough step length can ensure the global optimality and the stability of reconstruction, it suffers from high time cost. Therefore we introduce a coarse-to-fine search strategy in the alternate search scheme. We first search the value of density over the initial wide interval with a coarse step length to determine a rough approximate density. Then we define a smaller interval around the roughly determined value and search source density for another time with a finer step size. Considering the inertia of the digital representation type that the source domain hardly changes when the variation of density is fairly slight, we determine the source density by using one dimension search following the law of golden section to get a more reliable value after the determination of source domain.

When using the two-phase representation for BLT reconstruction, the solving domain is divided into two parts: source and background domain. For the latter, the source density is considered to be zero, and the expression of source distribution reduces to $S = s_0(1 - H(\varphi))$, where s_0 denotes the source density. So $\partial S/\partial\varphi = -s_0\delta(\varphi)$, and $dJ/dt = R'(S)^* R(S)(-s_0\delta(\varphi)f(\mathbf{r},t))$. Because s_0 is positive, the evolution law for two-phase representation is $f(\mathbf{r},t) = s_0 R'(S)^* R(S)$.

By adding additional alternate search of source density, the above alternate search algorithm for two-phase representation can be flexibly used in multi-phase case.

3. Numerical experiments

Numerical experiments based on a heterogeneous cylinder phantom are designed and performed to evaluate the performance of our reconstruction method. The phantom is 15 mm in radius and 30 mm in height, which is comparable to the chest of experimental mouse. Several tissues like volumes such as muscle, lungs, heart and bone are set in the phantom to model a mouse chest [14,16] as shown in Fig. 2. Optical parameters are shown in Table 1. They are calculated by optical tomography procedure and correspond to physical materials described in the following physical experiments [14]. Permissible region is set to $P = \{(x,y,z) : 8 < \sqrt{x^2+y^2} < 13, 13.5 < z < 16.5\}$ for the inverse source reconstruction.

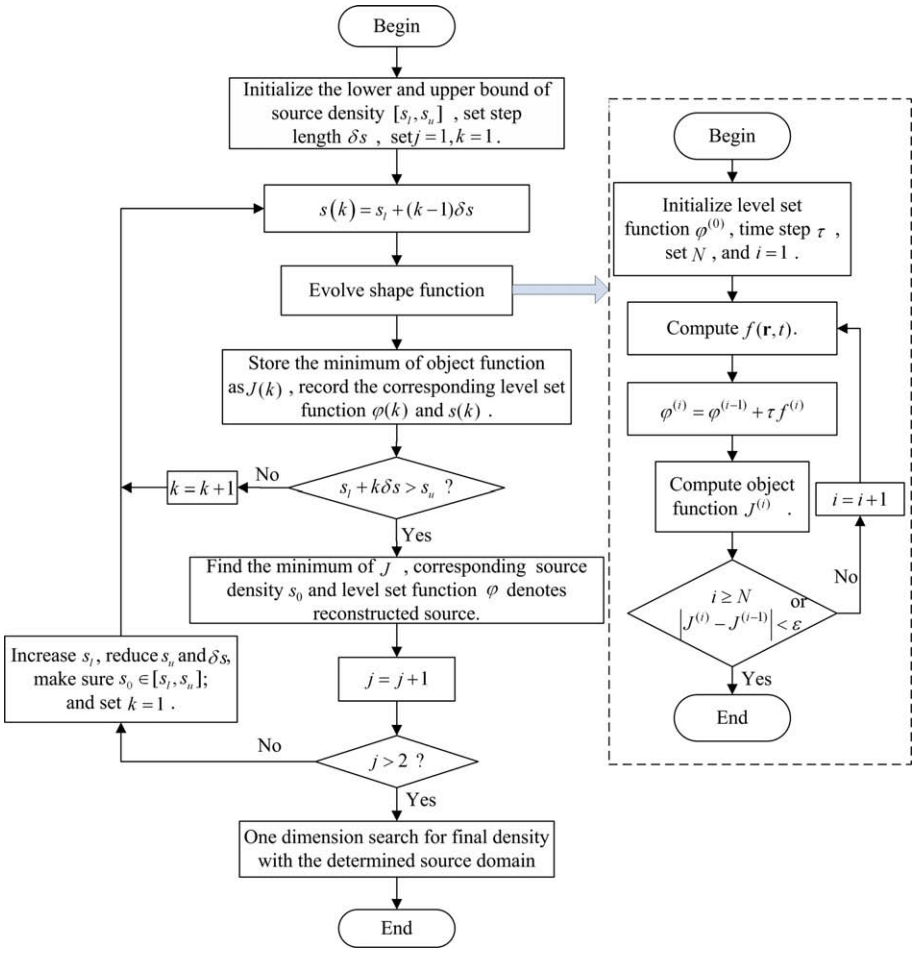

Fig. 1. Flow chart of the proposed algorithm.

In numerical simulations, the inverse reconstruction of bioluminescence source is usually based on synthetic surface measured data from the numerical solution of the forward problem. In order to avoid the *inverse crime*, different finite element methods including shape functions and meshes are adopted in the forward and inverse process [33]. In the forward calculation, a quadratic finite element method is used to compute the surface flux density with a mesh of 66,374 tetrahedral

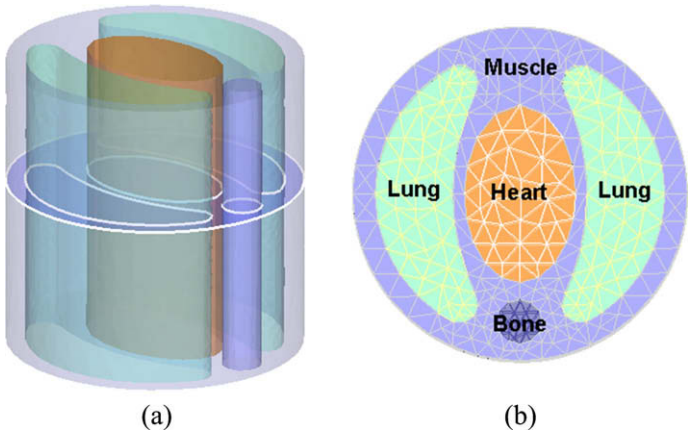

Fig. 2. Heterogeneous phantom (a) and its *x*-*y* view (b).

Table 1
Optical parameters of the heterogeneous phantom.

Material	Tissue	Lung	Heart	Bone
μ_a (mm^{-1})	0.007	0.023	0.011	0.001
μ_s'(mm^{-1})	1.031	2.000	1.096	0.060

elements and 11,988 nodes. This mesh is used in all the forward calculations of the numerical simulation in this paper. For all the reconstruction of numerical calculations the mesh has 5418 nodes and 28,548 elements.

3.1. Source detection

Two simulation experiments are performed in this section to verify the performance of the proposed reconstruction method on single source detection. In the first experiment, a sphere source of 1 mm radius is positioned at (−9, 0, 15) in the left lung with the power density of 1 nW/mm^3. In the second experiment a cube source of 2 mm on each side is centered at (−9, 0, 15), and its power density is the same as the first one. For the single source detection experiment and the stability analysis in Section 3.2 the two-phase representation is adopted, where the lower bound of s_0 is 0.01, the upper one is 1 and the step length 0.05 for the initial search. Artificial time step τ of level set reconstruction is set as 1. Initial domain indicated by level set function is set the same as permissible source domain. Maximum iterative number N and threshold ε are set as 500 and 0.001 respectively. For the first single source detection experiment, we obtain an approximate source density of 0.31 nW/mm^3 after the coarse search. According to the previously determined source density, we narrow down the value interval of s_0 from [0.01, 1] to [0.21, 0.41] and perform the fine search with step size 0.01. Then the final level set function and the corresponding reconstructed source location are obtained. By introducing the one dimension search for source density, the minimum value of Eq. (5) is 0.0069, and the reconstructed source density is 0.319 nW/mm^3. According to the final level set function, a reconstructed source centered at (−9.37, −0.07, 14.80) is determined, which is about 0.43 mm away from the actual one, as shown in Fig. 3(a). The distance error is calculated by $D = \|\mathbf{r}_{recons} - \mathbf{r_0}\|$, where $\mathbf{r}_{recons}$ is the reconstructed source center. As shown in Fig. 3(b), when the actual source is a cube, the reconstructed source is also centered at (−9.37, −0.07, 14.80) which is the same as the sphere source reconstruction, and the reconstructed source density is 0.641 nW/mm^3. Comparing the two experiments, we can make a conclusion that in order to reconstruct tiny bioluminescence source, we can neglect the reconstruction of source shape but focus on its localization and quantification.

Considering the *ill-posedness* of the inverse source problem that it is difficult to distinguish the influence of small source of high density and large one of weak density [28], reconstructed source power is selected as a quantitative index to evaluate the performance of the proposed method. Here we estimate the source power following the integral method by computing $\int S(\mathbf{r})d\mathbf{r}$ over the support of source. When the actual source is a sphere of 1 mm radius, the reconstructed result is 3.03 nW while the real value is 4.19 nW. Relative error between the actual one and the reconstructed one is 27.7%, according to $RE = |P_{real} - P_{recons}|/P_{real}$, where P_{real} is the actual power of source and P_{recons} denotes the reconstructed source power. For the second source detection experiment, the reconstructed power is 6.09 nW while the real value is 8 nW, hence the relative error is 23.9%. It is observed that the reconstructed source power is not accurate enough. This is mainly caused by two probable reasons. First, the accuracy of the inverse calculation based on FEM method needs to be improved. Refining the FEM mesh or using high-order interpolation function, we can obtain improved reconstructed power. However, the increment of element number or interpolation function order will heavily increase the computational burden. Second, source integral based power computation method depends on the topology information of source highly. It reduces the accuracy of quantification recon-

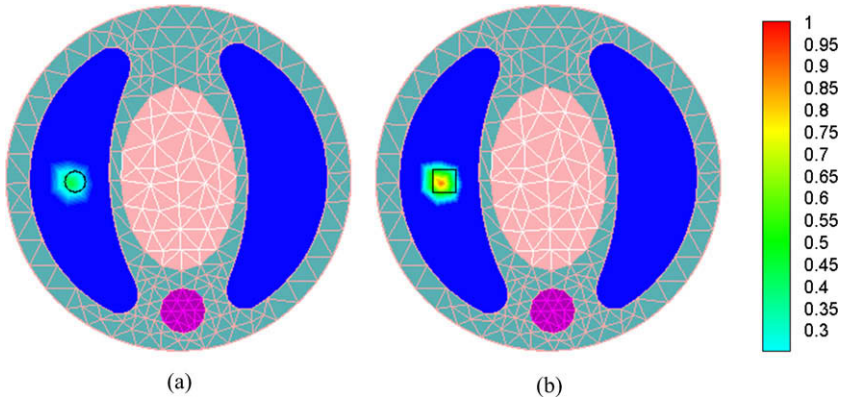

Fig. 3. Cross-section of normalized results of single source reconstruction at $z = 15$ mm, black lines in the left lungs denote actual position of sources: (a) actual source is a sphere of 1 mm radius; (b) actual source is a cube of 2 mm on each side.

struction. To avoid this problem, Jiang has proposed a new power computation method to compute the source power based on the moment of source, which has the ability of avoiding the influence of source topology [16]. However, this method is limited to sources that can be expressed by radial based function.

3.2. Stability analysis

We evaluate the stability and robustness of the reconstruction algorithm by considering the noise effect. Simulations based on synthetic surface measured data with different level (5%, 10%, 20%, 40%, 50% and 60%) of additive Gaussian noise are performed. Relationship between the minimum of objective function and the source density using the coarse-to-fine search method is shown in Fig. 4. The results indicate that the proposed method can successfully escape the local optimal solution and reach the global optimization even when the calculated data are influenced by noise. The results in Table 2 show that for an acceptable noise level (probably less than 40% for this experiment), our method can precisely locate the unknown source and quantify the source power stably. This advantage is achieved by the proposed source distribution representation method. In the proposed method, the distribution is represented by level set function in a digital form, where a slight change of source distribution may lead to an obvious variation of calculated surface flux density distribution. In other words, the source distribution is insensitive to the variation of surface signal distribution and is more stable to noise data. However, when the random noise is high, the data distribution on phantom surface may be disturbed heavily and the reconstructed result becomes bad as the noise level of 50%. In this case, the solution is trapped in local extremum, which directly affects the reconstructed results.

3.3. Source resolution

It is difficult to avoid the interference between multiple sources. In this section, groups of reconstruction experiments are performed to demonstrate the potential of the proposed method in sources resolution. And the results of the proposed method are compared with the classical modified Newton method used in [14,15,31]. For the Newton method, a Tikhonov regularization term $\lambda S^T S$ is added to the objective function (5) to reduce the *ill-posedness* of the reconstruction, and the regularization parameter λ is empirically set as 8×10^{-10}in the simulation. In the reconstruction of the proposed multiphase level set method, two level set functions which initially denote domains $P_1 = \{(x,y,z) \in P$, and $y > -1\}$ and $P_2 = \{(x,y,z) \in P$, and $y < 1\}$ respectively are adopted to represent the two different values of the interior source density. The corresponding source density s_1 and s_2 are both searched linearly over the interval [0.01,1] with the step length of 0.05 for the coarse search. Other parameters are set as the same as that in Section 3.1. Based on the heterogeneous phantom as shown in Fig. 2, two sphere sources labeled as S1 and S2 with the radius of 1 mm are positioned at (−9, 2.5, 15) and (−9, −2.5, 15). The density of S2 is set as 1 nW/mm^3 in the forward calculation and that of S1 is set as 0, 0.3, 0.5, 0.7 and 1 nW/mm^3 respectively. The corresponding power of S2 is 4.19 nW and 0, 1.26, 2.10, 2.93, 4.19 nW for S1. Reconstruction results of both the proposed level set method and the Newton method are shown in Figs. 5 and 6.

Five groups of reconstructed results are shown in Fig. 5. For convenience, the horizontal axis is defined as the power ratio which is calculated using the power of S1 divided by the power of S2. It is obvious that both the proposed algorithm and the Newton method can reconstruct the double sources when the power ratio varies from 0.5 to 1 in the simulations. However, there are some differences between these two methods. For the proposed algorithm, the reconstructed power of S1 increases

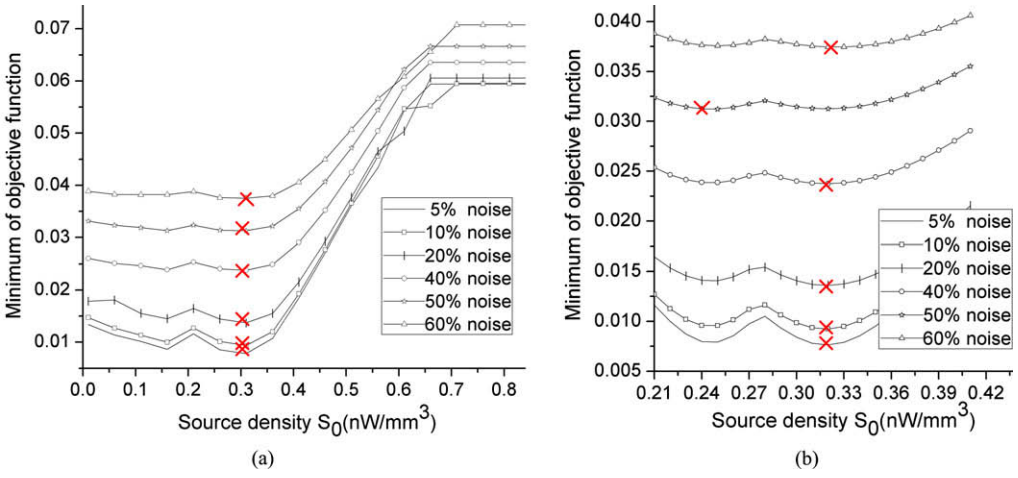

Fig. 4. Curve of the minimum of objective function corresponding to source density when different level of Gaussian noise is added to the measured data. The red crosses denote the minimums of the objective function: (a) results of the coarse search; (b) results of the fine search. For interpretation of colour in figures, the reader is referred to the Web version of this article.

Table 2
Reconstructed results of proposed algorithm under different level of noise data.

Noise level (%)	Source position (mm)		Reconstructed results		Minimum of objective function
	Actual	Reconstructed	D (mm)	Power (nW)	
5	(−9, 0, 15)	(−9.37,−0.07, 14.80)	0.43	3.03	0.75e−2
10	(−9, 0, 15)	(−9.37,−0.07, 14.80)	0.43	3.03	0.91e−2
20	(−9, 0, 15)	(−9.37,−0.07, 14.80)	0.43	3.07	1.36e−2
40	(−9, 0, 15)	(−9.37,−0.07, 14.80)	0.43	3.04	2.37e−2
50	(−9, 0, 15)	(−8.61, −1.00,14.91)	1.08	3.76	3.09e−2
60	(−9, 0, 15)	(−9.37,−0.07, 14.80)	0.43	3.19	3.7e−2

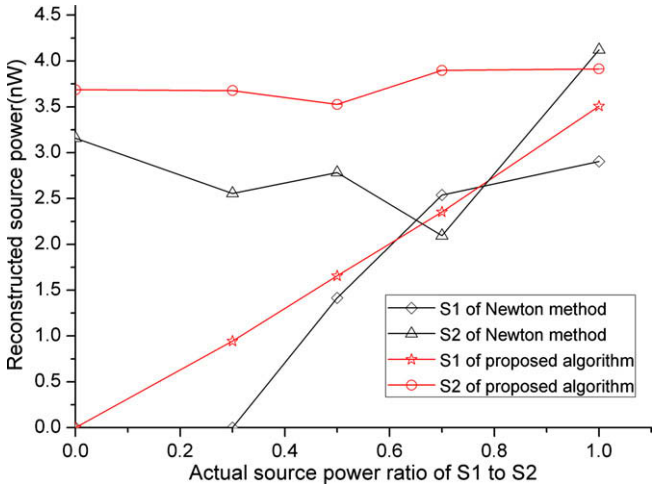

Fig. 5. Comparisons of reconstructed power between the proposed algorithm and Newton method.

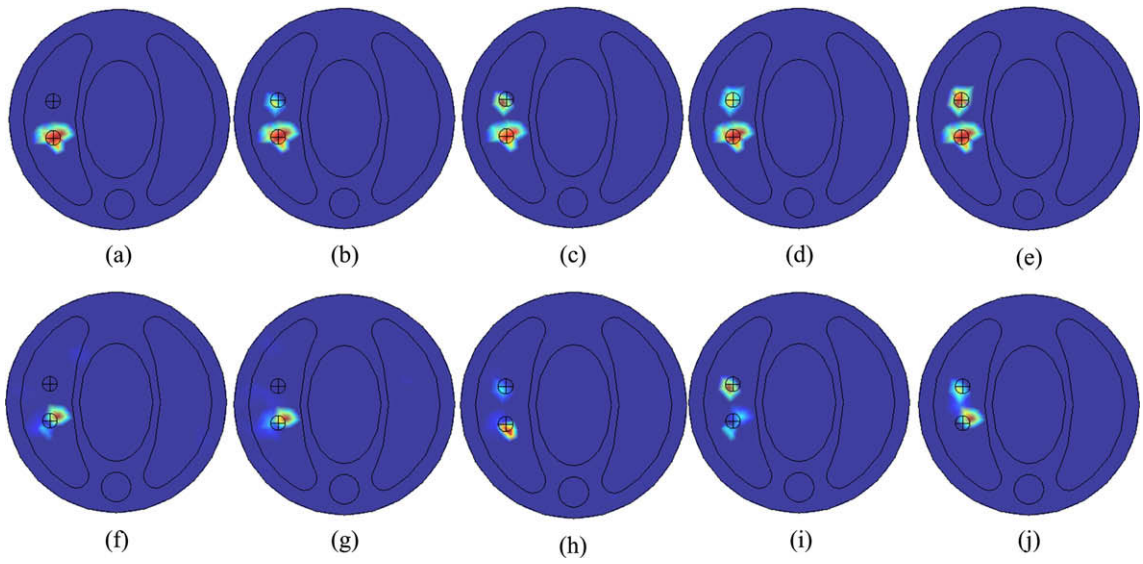

Fig. 6. Comparisons between the proposed algorithm and the Newton method on source location, the density of S1 is set as 0, 0.3, 0.5, 0.7 and 1 nW/mm^3 respectively and S2 is 1 nW/mm^3: (a)-(e) the results of multi-phase LSM reconstruction; (f)-(j) reconstructed results of Newton method.

steadily as its actual value varied and reconstructed power of S2 remains at the same level. But the results of Newton method are dramatically changed with the power ratio. From the cross-section of the reconstruction results shown in Fig. 6, we can find out that the reconstructed source location of S2 affected little by S1 for the proposed algorithm. But for the Newton method, the reconstructed S2 changes obviously when S1 is different. Moreover, when one source is much weaker than

the other one, for example when the power ratio is 0.3 in the simulation, the Newton method fails to resolve the weaker source while the proposed algorithm still works well. This is mainly caused by the different evolution mode of reconstruction methods. In the Newton method, the value of source density evolves directly. It is more sensitive to the surface signal distribution so that it suffers from low stability. Moreover, the reconstruction result of the Newton method often contains plenty of nonzero terms, which induces the difficulty of distinguishing source and background and decreases the resolution ability. However, source density in the proposed method evolves indirectly by updating the level set function. What is more, the expression of solution is in a more robust digital type, which contributes to eliminate the interference between different sources and guarantee the resolution ability of multiple sources.

4. Physical experiment

Physical experiment is performed in this section to demonstrate the validity of our reconstruction method. A heterogeneous cylindrical phantom of 30 mm height and 15 mm diameter is designed and manufactured. Four kinds of materials polyethylene, nylon, delrin and polypropylene are consisted in the phantom to present the muscle, lungs, heart and bone respectively. Two small holes of diameter 2 mm are drilled in the phantom to emplace the light sources, as shown in Fig. 7. Compound solutions of fluorescent dye from a red luminescent light stick are injected into the holes in the phantom to serve as the internal bioluminescent source. Inside the plastic light stick, there are two kinds of chemical solutions separated by a glass vial. By bending or shaking the stick, the inside glass vial will be broken and the two solutions are mixed. Then luminescent light whose central wavelength located about 650 nm is emitted. A back-thinned, back-illuminated cooled CCD camera (Princeton Instruments PIXIS 2048B) is adopted to measure the signal on the phantom surface from four views by rotating the phantom with an angular increment of 90 degrees. Fig. 8 (a)-(d) show the corresponding measured data on CCD. In order to reconstruct the interior source, the collected data on the CCD plane are mapped to the three-dimensional phantom surface by considering the photon transmission in free space [36]. The normalized flux density distribution on the phantom surface is adopted to localize the unknown source. The optical parameters of the material include in the phantom calculated by optical tomography are listed in Table 1.

The center positions of actual sources are $(-9, 2, 16.6)$ and $(-9, -3, 16.6)$ respectively. A permissible region of source as $\{(x, y, z) : 8 < \sqrt{x^2 + y^2} < 13, 15 < z < 18\}$ is adopted in the reconstruction according to the flux density distribution on

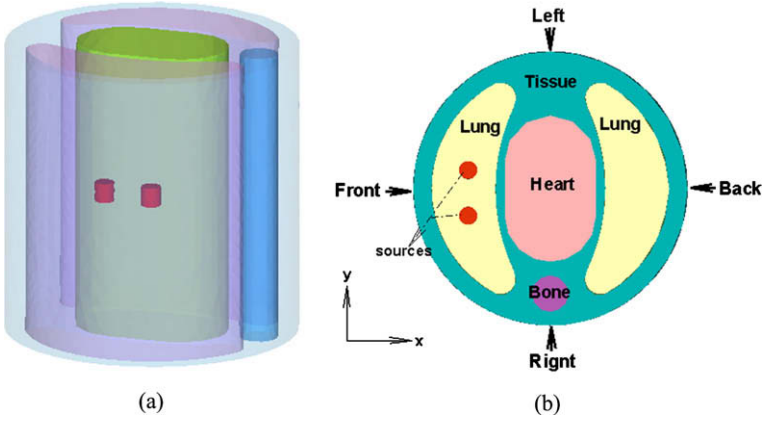

Fig. 7. Physical phantom and its x-y view at $z = 16.6$ mm.

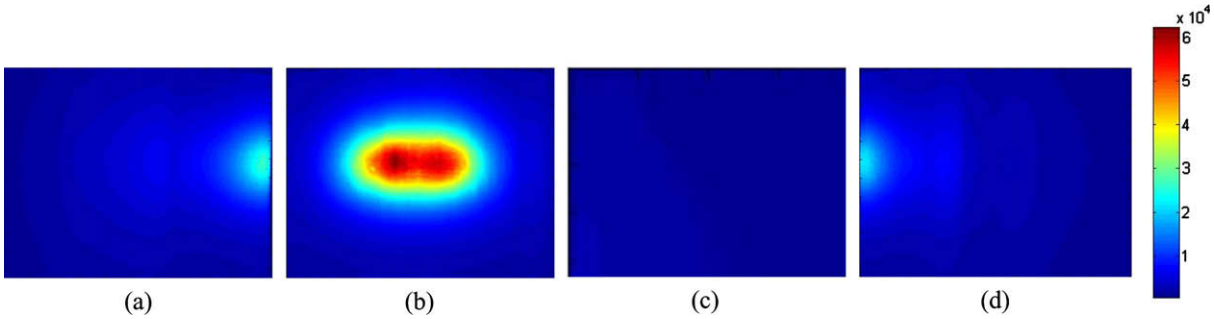

Fig. 8. Four views of CCD measured data: (a) left view; (b) front view; (c) back view; (d) right view.

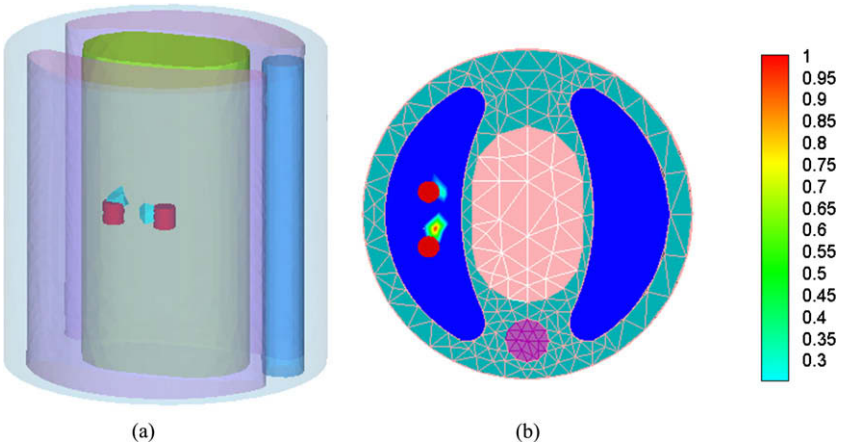

Fig. 9. Normalized results of physical phantom reconstruction: (a) 3D view of reconstruction result; (b) corresponding cross-section at $z = 16.6$ mm.

phantom surface. The finite element mesh adopted for reconstruction has 5490 nodes and 29,476 tetrahedron elements. Fig. 9 shows the reconstructed result, where the red cylinders denote the actual sources and the small domains around the cylinders represent the reconstructed sources. From the 3D view of reconstructed results and its corresponding cross-section, we can find out that the reconstructed sources recover the real ones well. The reconstructed source positions are $(-8.09, 2.01, 17.57)$ and $(-8.38, -1.34, 16.64)$, which are 1.33 mm and 1.78 mm away from the actual ones respectively.

5. Conclusion

We develop a novel multi-phase level set method for the bioluminescent source reconstruction. The level set representation makes the reconstruction highly robust and of high quality for multiple sources resolution. The alternate search scheme ensures the global optimum and the stability of the solution. Numerical and physical phantom experiments prove the potential of the proposed method in localization and quantification for phantom based BLT source reconstruction. The efficiency and flexibility of the proposed method needs to be improved further for practical application. Parallel computation strategy may be incorporated for computation acceleration and more efficient search method should be developed.

Acknowledgments

This work is supported by the Program of the National Basic Research and Development Program of China (973) under Grant No. 2006CB705700, the Cheung Kong Scholars and Innovative Research Team in University (PCSIRT) under Grant No. IRT0645, the Chair Professors of Cheung Kong Scholars Program of Ministry of Education of China, CAS Hundred Talents Program, the National Natural Science Foundation of China under Grant Nos. 30873462, 60532050, 30900334, the Beijing Municipal Natural Science Foundation of China under Grant No. 4071003, the CAS Scientific Research Equipment Develop Program (YZ0642, YZ200766), the Shaanxi Provincial Natural Science Foundation Research Project under Grant No. 2009JQ8018.

References

[1] V. Ntziachristos, J. Ripoll, L.V. Wang, R. Weisslder, Looking and listening to light: the evolution of whole body photonic imaging, Nat. Biotechnol. 23 (2005) 313–320.
[2] J.K. Willmann, N. van Bruggen, L.M. Dinkelborg, S.S. Gambhir, Molecular imaging in drug development, Nature 7 (2008) 591–607.
[3] G. Wang, E.A. Hoffman, G. McLennan, L.V. Wang, M. Suter, J. Meinel, Development of the first bioluminescent CT scanner, Radiology 229 (2003) 566.
[4] J. Tian, J. Bai, X.P. Yan, S.L. Bao, Y.H. Li, W. Liang, X. Yang, Multimodality molecular imaging, IEEE EMB Mag. 27 (2008) 48–57.
[5] G. Wang, W. Cong, K. Durairaj, X. Qian, H. Shen, P. Sinn, E. Hoffman, G. McLennan, M. Henry, In vivo mouse studies with bioluminescence tomography, Opt. Express 14 (2006) 7801–7809.
[6] A.D. Klose, V. Ntziachristos, A.H. Hielscher, The inverse source problem based on the radiative transfer equation in optical molecular imaging, J. Comput. Phys. 202 (2005) 323–345.
[7] Y. Lv, A.F. Chatziioannou, A parallel adaptive finite element method for the simulation of photon migration with the radiative-transfer-based model, Commun. Numer. Meth. Engng. (2008), doi:10.1002/cnm.1167.
[8] W. Cong, A. Cong, H. Shen, Y. Liu, G. Wang, Flux vector formulation for photon propagation in the biological tissue, Opt. Lett. 32 (2007) 2837–2839.
[9] S.R. Arridge, M. Schweiger, M. Hiraoka, D.T. Delpy, A finite element approach for modeling photon transport in tissue, Med. Phys. 20 (1993) 299–309.
[10] J. Ripoll, D. Yessayan, G. Zacharakis, V. Ntziachristos, Experimental determination of photon propagation in highly absorbing and scattering media, J. Opt. Soc. Am. A 22 (2005) 546–551.
[11] T.J. Farrell, M.S. Patterson, B. Wilson, A diffusion theory model of spatially resolved, steady-state diffuse reflectance for the noninvasive determination of tissue optical properties in vivo, Med. Phys. 19 (1992) 879–888.
[12] Y. Hou, J. Tian, Y. Wu, J. Liang, X. He, A new numerical method for BLT forward problem based on high-order finite elements, Commun. Numer. Meth. Engng. (2008), doi:10.1002/cnm.1202.

[13] W. Cong, D. Kumar, Y. Liu, A. Cong, G. Wang, A practical method to determine the light source distribution in bioluminescent imaging, Proc. SPIE 5535 (2004) 679–686.
[14] W. Cong, G. Wang, D. Kumar, Y. Liu, M. Jiang, L.V. Wang, E.A. Hoffman, G. McLennan, P.B. McCray, J. Zabner, A. Cong, Practical reconstruction method for bioluminescence tomography, Opt. Express 13 (2005) 6756–6771.
[15] Y. Lv, J. Tian, W. Cong, G. Wang, J. Luo, W. Yang, H. Li, A multilevel adaptive finite element algorithm for bioluminescence tomography, Opt. Express 14 (2006) 8211–8223.
[16] M. Jiang, T. Zhou, J. Cheng, W. Cong, G. Wang, Image reconstruction for bioluminescence tomography from partial measurement, Opt. Express 15 (2007) 11095–11116.
[17] N. Slavine, M. Lewis, E. Richer, P. Antich, Iterative reconstruction method for light emitting sources based on the diffusion equation, Med. Phys. 33 (2006) 61–68.
[18] S. Ahn, A.J. Chauhari, F. Darvas, C.A. Bouman, R.M. Leahy, Fast iterative image reconstruction methods for fully 3D multispectral bioluminescence tomography, Phys. Med. Biol. 53 (2008) 3921–3942.
[19] S.J. Osher, J.A. Sethian, Fronts propagating with curvature dependent speed: algorithms based on Hamilton–Jacobi formulations, J. Comput. Phys. 79 (1988) 12–49.
[20] T.F. Chan, X.C. Tai, Level set and total variation regularization for elliptic inverse problems with discontinuous coefficients, J. Comput. Phys. 193 (2003) 40–66.
[21] O. Dorn, D. Lesselier, Level set methods for inverse scattering, Inverse Probl. 22 (2006) R67–R131. Topical Review.
[22] K. van den Doel, U.M. Ascher, Dynamic level set regularization for large distributed parameter estimation problems, Inverse Probl. 23 (2007) 1271–1288.
[23] T.F. Chan, H. Li, M. Lysaker, X.-C. Tai, Level set method for positron emission tomography, Int. J. Biomed. Imaging (2007) 26950, doi:10.1155/2007/26950.
[24] N. Irishina, O. Dorn, M. Moscoso, A level set evolution strategy in microwave imaging for early cancer detection, Comput. Math. Appl. 56 (2008) 607–618.
[25] E.T. Chung, T.F. Chan, X.-C. Tai, Electrical impedance tomography using level set representation and total variational regularization, J. Comput. Phys. 205 (2005) 357–372.
[26] M.E. Kilmer, E.L. Miller, A. Barbaro, D. Boas, Three-dimensional shape-based imaging of absorption perturbation for diffuse optical tomography, Appl. Opt. 42 (2003) 3129–3144.
[27] M. Schweiger, S.R. Arridge, Reconstructing absorption and diffusion shape profiles in optical tomography by a level set technique, Opt. Lett. 31 (2006) 471–473.
[28] V.Y. Soloviev, Tomographic bioluminescence imaging with varying boundary conditions, Appl. Optics 46 (2007) 2778–2784.
[29] W. Rice, M.D. Cable, M.B. Nelson, In vivo imaging of light-emitting probes, J. Biomed. Opt. 6 (2001) 432–440.
[30] M. Schweiger, S.R. Arridge, M. Hiraoka, D.T. Delpy, The finite element method for the propagation of light in scattering media: boundary and source conditions, Med. Phys. 22 (1995) 1779–1792.
[31] J. Feng, K. Jia, G. Yan, S. Zhu, C. Qin, Y. Lv, J. Tian, An optimal permissible source region strategy for multispectral bioluminescence tomography, Opt. Express 16 (2008) 15640–15654.
[32] L.A. Vese, T.F. Chan, A new multiphase level set framework for image segmentation via the Mumford and Shah model, Int. J. Comput. Vision 50 (2002) 271–293.
[33] D.L. Colton, R. Kress, Inverse Acoustic and Electromagnetic Scattering Theory, second ed., Springer, Berlin, New York, 1998. p. 304.
[34] N.M. Tanushev, L.A. Vese, A piecewise-constant binary model for electrical impedance tomography, Inverse Prob. Imaging (IPI) 1 (2007) 423–435.
[35] T.F. Chan, L.A. Vese, Active contours without edges, IEEE Trans. Image Process. 10 (2001) 266–277.
[36] X. Chen, X. Gao, X. Qu, J. Liang, L. Wang, D. Yang, A. Garofalakis, J. Ripoll, J. Tian, A study of phonton propagation in free-space based on hybrid radiosity-radiance theorem, Opt. Express 17 (2009) 16266–16280.